Key Points:
- The substorm-electron injection peeled off the nightside plasmasphere and excited the chorus outside the plasmapause
- The azimuthally drifting hot electrons intensified the plasmaspheric hiss gradually from nightside to dayside
- The nightside large-amplitude hiss might be generated by the hot electrons drifting into the outer plasmasphere

Supporting Information:
- Supporting Information S1

Multipoint Observations of Nightside Plasmaspheric Hiss Generated by Substorm-Injected Electrons

Zhenpeng Su[1,2] (ID), **Nigang Liu**[1,2,3] (ID), **Huinan Zheng**[1,2] (ID), **Yuming Wang**[1,2] (ID), **and Shui Wang**[1,2]

[1]CAS Key Laboratory of Geospace Environment, Department of Geophysics and Planetary Sciences, University of Science and Technology of China, Hefei, China, [2]Collaborative Innovation Center of Astronautical Science and Technology, University of Science and Technology of China, Hefei, China, [3]Mengcheng National Geophysical Observatory, School of Earth and Space Sciences, University of Science and Technology of China, Hefei, China

Abstract Plasmaspheric hiss plays a key role in shaping the radiation belt environment, whose origin remains under active debate. Using the wave and particle data of Van Allen Probes, Geostationary Operational Environmental Satellites, and Time History of Events and Macroscale Interactions during Substorm spacecraft, we here examine the nightside plasmaspheric hiss generation during a substorm. The substorm-electron injection caused the plasmapause to shrink promptly from $L_{pp} = 6.6$ to 5.1. Corresponding to the azimuthal drift of the injected electrons, the plasmaspheric hiss was intensified gradually from nightside to dayside. Particularly, in the inner postmidnight plasmasphere free from the substorm injection, the instantaneous peak amplitude of hiss reached 0.9 nT. The enhanced hiss within the locally unchanged plasma must originate from other spatial regions. Our data and modeling demonstrate that the large-amplitude hiss was generated by the substorm-injected electrons drifting into the outer postmidnight plasmasphere, rather than linked to the nightside chorus suffering strong Landau damping or the dayside chorus/hiss propagating azimuthally to the nightside plasmasphere.

Plain Language Summary Plasmaspheric hiss, a naturally occurring electromagnetic emission (0.1–2.0 kHz) in the dense cold plasma surrounding the Earth, can precipitate energetic electrons from the Van Allen radiation belts into the atmosphere. Since its discovery in 1969, the origin of plasmaspheric hiss has remained a puzzle to be solved. We here use the data of seven magnetospheric spacecraft to investigate the nightside plasmaspheric hiss generation during a substorm. Corresponding to the azimuthal drift of substorm-injection front, the plasmaspheric hiss is found to be intensified gradually from nightside to dayside. In the inner nightside plasmasphere free from the substorm injection, the instantaneous peak amplitude of hiss is shown to increase from less than 40 pT to 0.9 nT. Within the locally unchanged plasma, the substorm-enhanced hiss must originate from other spatial regions. Our data and modeling support the previously proposed hypothesis that the nightside hiss is excited by the hot electrons in the outer plasmasphere and then propagates to the inner plasmasphere. This experimental confirmation will allow further developments in modeling and forecasting of the plasmaspheric hiss spatiotemporal distribution and the Earth's radiation belt behavior.

1. Introduction

Plasmaspheric hiss is of particular importance for the precipitation loss of energetic electrons in the inner magnetosphere (e.g., Abel & Thorne, 1998; Albert, 1994; Lyons & Thorne, 1973; Mourenas & Ripoll, 2012; Ni et al., 2013, 2014; Summers et al., 2007). It can create the radiation belt slot during quite times and partially explain the outer radiation belt dropout during disturbed times (e.g., Breneman et al., 2015; Falkowski et al., 2017; He et al., 2016; Meredith et al., 2007; Ni et al., 2017; Shprits et al., 2009; Su et al., 2016; Thorne et al., 2013). Plasmaspheric hiss naturally occurs in the high-density plasmasphere and plasmaspheric drainage plume (Li, Ma. et al., 2015; Malaspina et al., 2017; Meredith et al., 2018; Russell et al., 1969; Summers et al., 2008; Thorne et al., 1973; Tsurutani et al., 2015), and its accurate generation mechanism remains controversial. There have been proposed two classes of physical scenarios: one involves the linear or nonlinear instability of hot electrons inside the plasmasphere and plasmaspheric drainage plume (*internal excitation*; Chen et al., 2014; Cornilleau-Wehrlin et al., 1993; Li et al., 2013; Omura et al., 2015; Solomon et al., 1988; Summers et al., 2014; Thorne et al., 1979); the other envisions lightning-associated whistlers (Draganov et al., 1992; Green et al., 2005;

Sonwalkar & Inan, 1989) or whistler-mode chorus (Bortnik et al., 2008; Santolík & Chum, 2009) as embryonic sources (*external origination*).

In recent years, many experimental examinations of the plasmaspheric hiss generation have been conducted in the dayside and duskside magnetosphere. The external origination mechanism likely plays a dominant role in the plasmasphere body, as supported by the one-to-one correlation of hiss and chorus with an appropriate time lag (Bortnik et al., 2009; Li, Chen, et al., 2015; Wang et al., 2011), the opposite Poynting fluxes of hiss and chorus at low altitudes (Tsurutani et al., 2012), the clear gap of 1–2 Earth radii between hiss and chorus further out (Malaspina et al., 2016; Meredith et al., 2013), and the simultaneous disappearances of hiss and chorus following interplanetary disturbances (Liu, Su, Gao, Reeves, et al., 2017; Liu, Su, Gao, Zheng, et al., 2017; Su et al., 2015; Yue et al., 2017). In contrast, the internal excitation mechanism is required to account for the poleward Poynting fluxes (Laakso et al., 2015; Su et al., 2018) and the discrete rising tones of hiss on a timescale of 1 s (Su et al., 2018) within the plasmaspheric drainage plume.

However, there have been few studies performed to experimentally address the nightside plasmaspheric hiss generation mechanism. Tsurutani et al. (2015) believed that the nightside chorus is unable to access the plasmasphere because of strong Landau damping and that the nightside hiss is generated directly by the substorm-injected hot electrons inside the plasmasphere (Chen et al., 2014; Meredith et al., 2004; Santolík et al., 2001; Thorne et al., 1979). Chen et al. (2009) suggested that the dayside chorus can enter the plasmasphere and then propagate azimuthally into the nightside region. In this letter, we present an experimental test on the generation of nightside plasmaspheric hiss during an isolated substorm, made with the Van Allen Probes (RBSP; Mauk et al., 2013), the Geostationary Operational Environmental Satellites (GOES; Davis, 2007), and the Time History of Events and Macroscale Interactions during Substorm (THEMIS) spacecraft (Angelopoulos, 2008) on 16 December 2016.

2. Spacecraft and Instrumentation

The OMNI database of CDAweb (King & Papitashvili, 2005) provided interplanetary and geomagnetic parameters, and the RBSP, GOES, and THEMIS missions measured magnetospheric particles, fields, and waves. The RBSP mission was launched on 30 August 2012, comprising two identical probes (RBSP-A and RBSP-B) in the highly elliptical orbits with geocentric distances of $\sim$1.1 R_E at perigees and $\sim$6.0 R_E at apogees. The Electric and Magnetic Field Instrument and Integrated Science (EMFISIS) suite (Kletzing et al., 2013) and the Helium Oxygen Proton Electron (HOPE; Funsten et al., 2013) and the Magnetic Electron Ion Spectrometer (MagEIS; Blake et al., 2013) of the Energetic Particle, Composition, and Thermal Plasma Suite (ECT; Spence et al., 2013) are used here. To accomplish the GOES mission, GOES-13 and GOES-15 satellites were launched into the geostationary orbit with a geocentric distance of 6.6 R_E on 24 May 2006 and 4 March 2010. They were located at 75° and 135° geographic west longitude in the time range of interest, and only the Magnetospheric Electron Detector (MagED; GOES N Series Data Book, 2009) is used. The THEMIS mission began on 17 February 2007 and consisted of five identical spacecraft. After Spring 2010, two spacecraft (TH-B and TH-C) moved into lunar orbits, and three spacecraft (TH-A, TH-D, and TH-E) remained in Earth orbits with geocentric distances of $\sim$1.5 R_E at perigees and $\sim$10.0 R_E at apogees. The Fluxgate Magnetometer (FGM; Auster et al., 2008), the Digital Fields Board (DFB; Cully, Ergun, et al., 2008), the Electrostatic Analyzer (ESA; McFadden et al., 2008), and the Solid State Telescope (SST; Angelopoulos, 2008) are used. The seven spacecraft with comprehensive instrumentation together enable simultaneous coverage over a very broad region and allow a detailed investigation of the nightside hiss generation during substorm.

3. Event Overview

Figure 1 shows the global plasmasphere dynamics on 16 December 2016. During 11:00–15:00 UT, the sustained intense southward interplanetary magnetic field directly triggered a substorm with the maximum $AE \approx 900$ nT. In the preceding $\sim$12 hr and the following $\sim$5 hr, the magnetosphere was quiescent with $AE < 100$ nT. The plasmapause generally results from the balance between the corotation and convection electric fields (e.g., Carpenter & Anderson, 1992; Goldstein et al., 2004; Lemaire & Gringauz, 1998; Nishida, 1966; Pierrard et al., 2008) and coincides with the transition layer of hot particles particularly during quiet times (Friedel et al., 2001; Horwitz et al., 1990; Li et al., 2010). Before the substorm, the plasmasphere extended to close to $L = 6.6$ in both midnight and dawn sectors, as observed by THEMIS mission. Correspondingly, RBSP mission immersed in the plasmasphere detected no steep gradient in the background electron den-
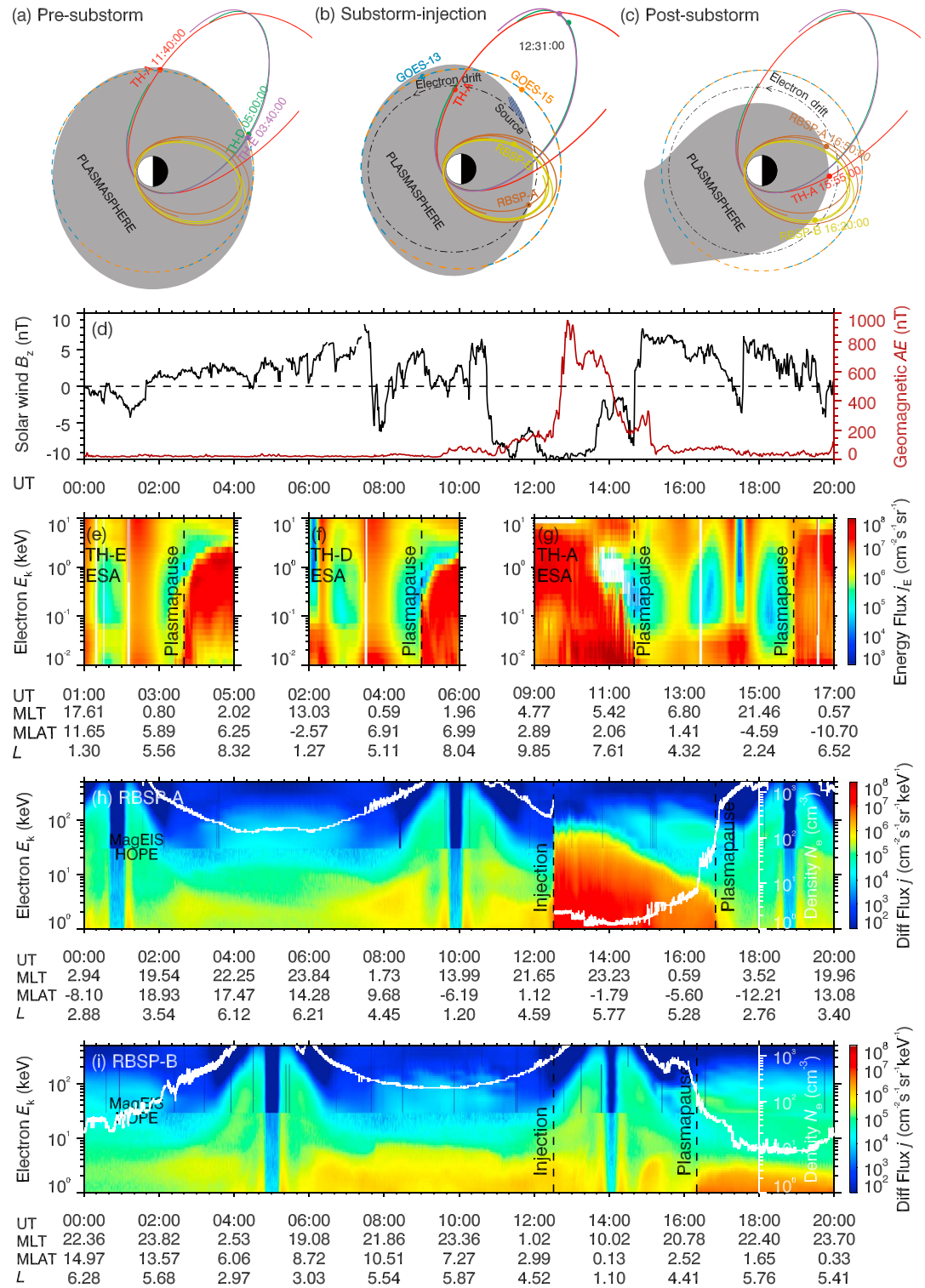
Figure 1. Plasmasphere dynamics observed by THEMIS and RBSP missions. (a–c) Schematic diagrams of plasmasphere structures (shadows), spacecraft orbits (colored lines), and hot electron drift paths (black dash-dotted lines) at three stages; (d) solar wind magnetic field B_z and substorm index AE; (e–g) plasmapause location L_{pp} identified as hot electron transition layer; (h and i) hot electron spin-averaged differential flux j and plasmapause location L_{pp} identified as the sharp gradient in the cold electron density N_e which is derived from the upper hybrid resonance frequency (Kurth et al., 2014). MLT = magnetic local time; MLAT = magnetic latitude.

sity. For GOES mission, there were no available data to determine its accurate location with respect to the plasmapause. At 12:31 UT (L = 5.1 and MLT = 22:07), the substorm-injection boundary (Friedel et al., 1996; McIlwain, 1974; Reeves et al., 1990) reached RBSP-A, enhancing the electron fluxes simultaneously over a wide energy range from ~10 eV to 200 keV and peeling off the nightside plasmasphere (Chappell, 1974; Lemaire & Gringauz, 1998). But at the same time, RBSP-B did not observe the hot electron injection nor the plasmapause reformation at inner shells of the postmidnight magnetosphere (L = 3.9 and MLT = 01:40). After the enhanced convection by the substorm, the shrinking plasmapause was encountered successively by TH-A at 15:55 UT (L = 4.5 and MLT = 23:40), by RBSP-B at 16:20 UT (L = 4.8 and MLT = 21:08), and by RBSP-A at 16:50 UT (L = 4.5 and MLT = 01:21).

Figure 2 gives the evolution of magnetospheric waves driven by the substorm. The singular value decomposition technique (Santolík et al., 2003) is applied on the spectral matrix to estimate the wave normal angle and polarization (Santolík et al., 2002). The cross-power spectra between components of the electric and magnetic fields are used to calculate the wave Poynting flux (Santolík et al., 2010). The quiet-time hiss occurred in the frequency range from 60 Hz to 1 kHz, with quite low power, right-hand polarizations, and bidirectional Poynting fluxes. These waves tended to propagate quasi-parallel to the magnetic field lines near the magnetic equator but become highly oblique at higher latitudes. Outside the premidnight newly formed plasmapause (RBSP-A), the substorm-injected hot electrons locally excited the whistler-mode chorus waves around 0.5 f_{ce} with the Poynting fluxes flowing away from the equator. At the inner shells of the postmidnight plasmasphere free from the hot electron injection (RBSP-B), the plasmaspheric hiss waves exhibited a prompt enhancement in the magnetic power by up to two orders of magnitude, which should originate from other spatial regions. In the next ~1 hr of the inbound pass, RBSP-B continuously collected the intense hiss signals with the similar polarization and propagation features to the quiet-time hiss. During the following outbound pass of RBSP-B (14:00–16:20 UT), only a few weak hiss emissions were observable in the premidnight sector. When RBSP-A went back into the postmidnight plasmasphere after 16:50 UT, the hiss power had fallen back to the quiet-time level. Note that the intense linearly polarized signals below 100 Hz were magnetosonic waves (Horne et al., 2007) associated with the substorm proton injection (Su et al., 2017).

4. Discussions

4.1. Potential Connection Between Nightside Hiss and Chorus

Figure 3 plots the nightside burst-mode hiss and chorus waves before and during the substorm. The hiss signals appeared to be structureless on the plotted timescale. During quiet time, their instantaneous amplitudes were below <40 pT, and the corresponding power spectral densities were comparable to those of the lightening whistlers (>1 kHz) with descending tones on a timescale of 1 s. In contrast, the hiss instantaneous amplitudes during the substorm frequently exceeded 0.5 nT and even reached 0.9 nT. If the enhanced hiss centering 0.2 kHz originated directly from the nightside chorus, the envisioned embryonic sources would be located around L = 8, beyond the spatial coverage of RBSP mission. Previous statistical study (Li et al., 2009) has shown that the amplitudes of nightside chorus tend to peak at $L < 7$. The largest amplitudes of chorus waves reported to date have been several nT in the inner magnetosphere (e.g., Cattell et al., 2008; Cully, Bonnell, et al., 2008; Kellogg et al., 2011; Gao et al., 2016; Santolík et al., 2014; Wilson et al., 2011). For this specific event, the observed chorus waves at L = 5.5 exhibited regular packets with the instantaneous peak amplitude of 1.0 nT. These results suggest that the nightside hiss and chorus had comparable amplitudes during this substorm and that the nightside chorus experiencing strong Landau damping was unlikely to become the large-amplitude hiss (Tsurutani et al., 2015).

4.2. Potential Connection Between Nightside and Dayside Hiss

Figure 4 displays the movement of substorm-injection front and the response of magnetospheric waves observed by GOES and THEMIS missions. Because GOES mission operated at higher magnetic shells than RBSP mission, the two missions were actually observing the different electron populations injected by the same substorm. GOES-15 and GOES-13 successively encountered this substorm-injection front at 12:30 UT (MLT = 03:30) and at 12:40 UT (MLT = 07:40). This substorm injection caused the hot electron fluxes to increase by up to 70 times. Because of the energy-dependent drift velocity, the electron injection became more dispersive at a more eastward MLT. The time delay between 40- and 125-keV electron flux peaks was ~25 min for GOES-15 and increased to ~40 min for GOES-13. For TH-A, there was no substorm-injection signature but an obvious intensification of plasma waves in the frequency range of 30–700 Hz after 12:40 UT (L = 5.0 and MLT = 06:25). This wave intensification timing was quite close to the electron injection timing of GOES-13.
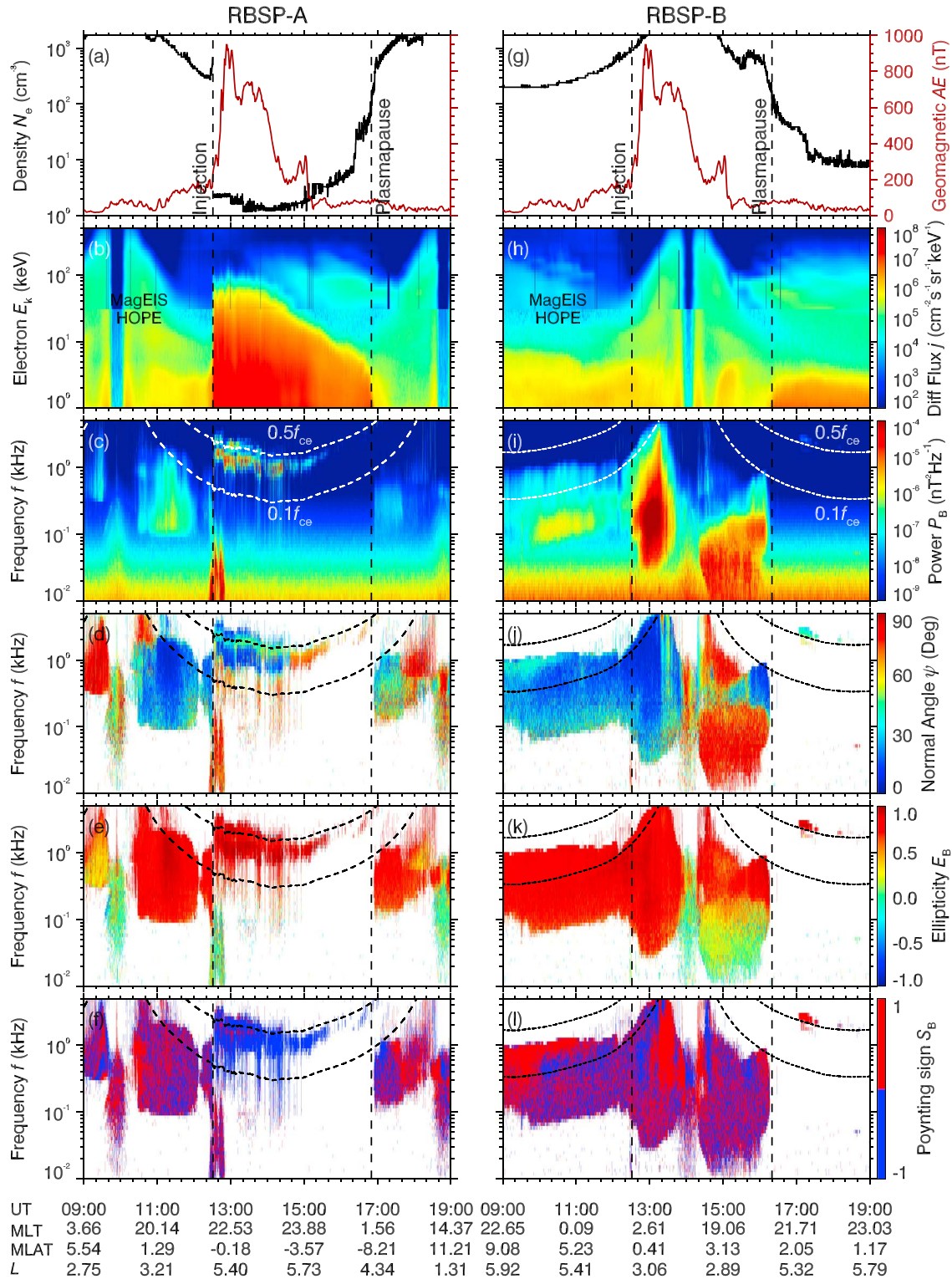
Figure 2. Substorm effect on magnetospheric waves observed by RBSP mission. (a and g) Cold electron density N_e and substorm index AE; (b and h) hot electron spin-averaged differential flux j, (c and i) wave power spectral density P_B, (d and j) wave normal angle ψ, (e and k) wave ellipticity E_B (negative for left-hand polarized waves and positive for right-handed ones), and (f and l) sign of field-aligned Poynting flux component S_B (positive for parallel flowing and negative for antiparallel flowing). The vertical-dashed lines mark the substorm-electron injection front and the plasmapause with a steep density gradient.
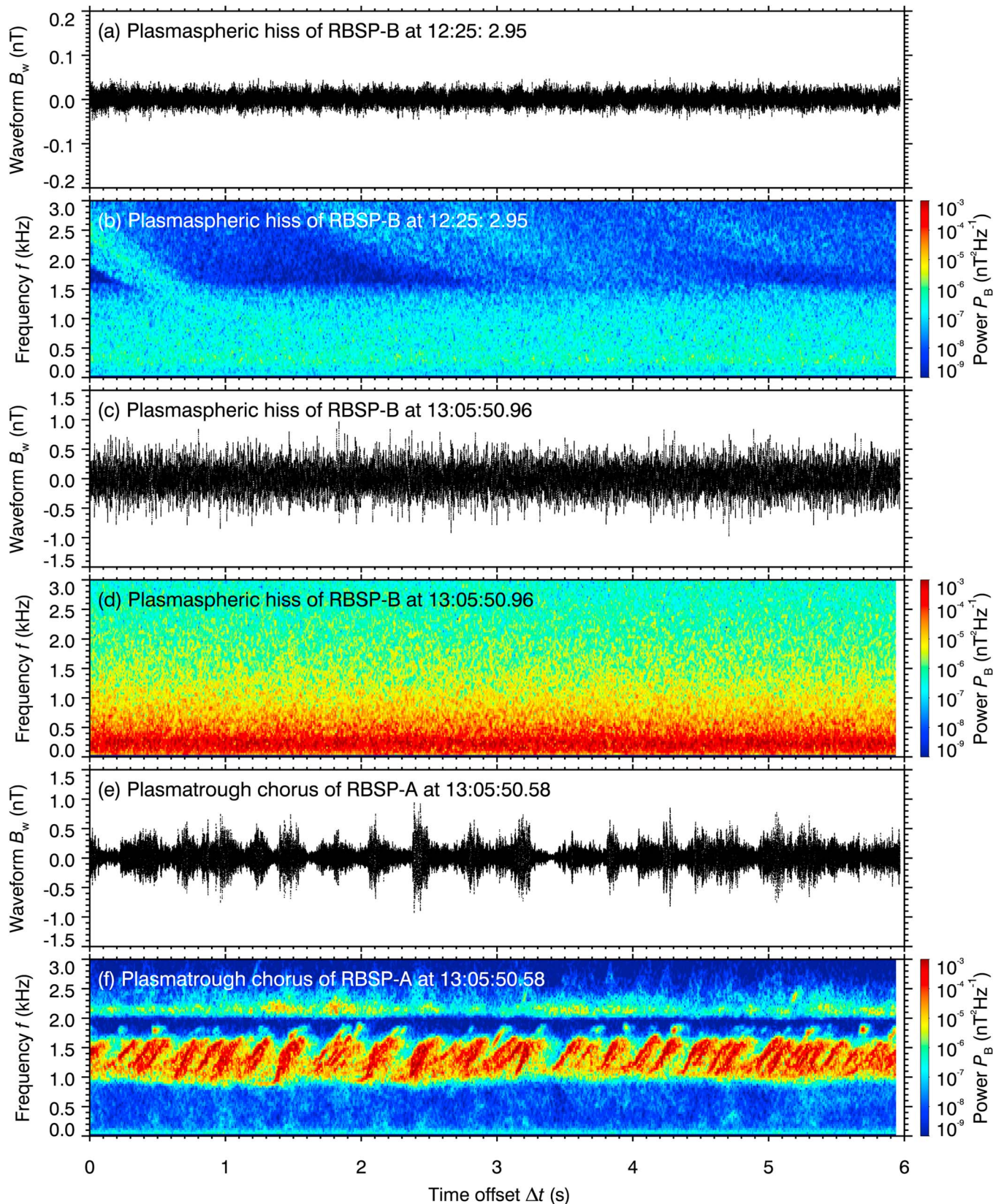
Figure 3. Burst-mode hiss and chorus waves observed by RBSP mission. (a, c, and e) Magnetic field component B_w in the nominal science payload coordinate system; (b, d, and f) wave power spectral density P_B.
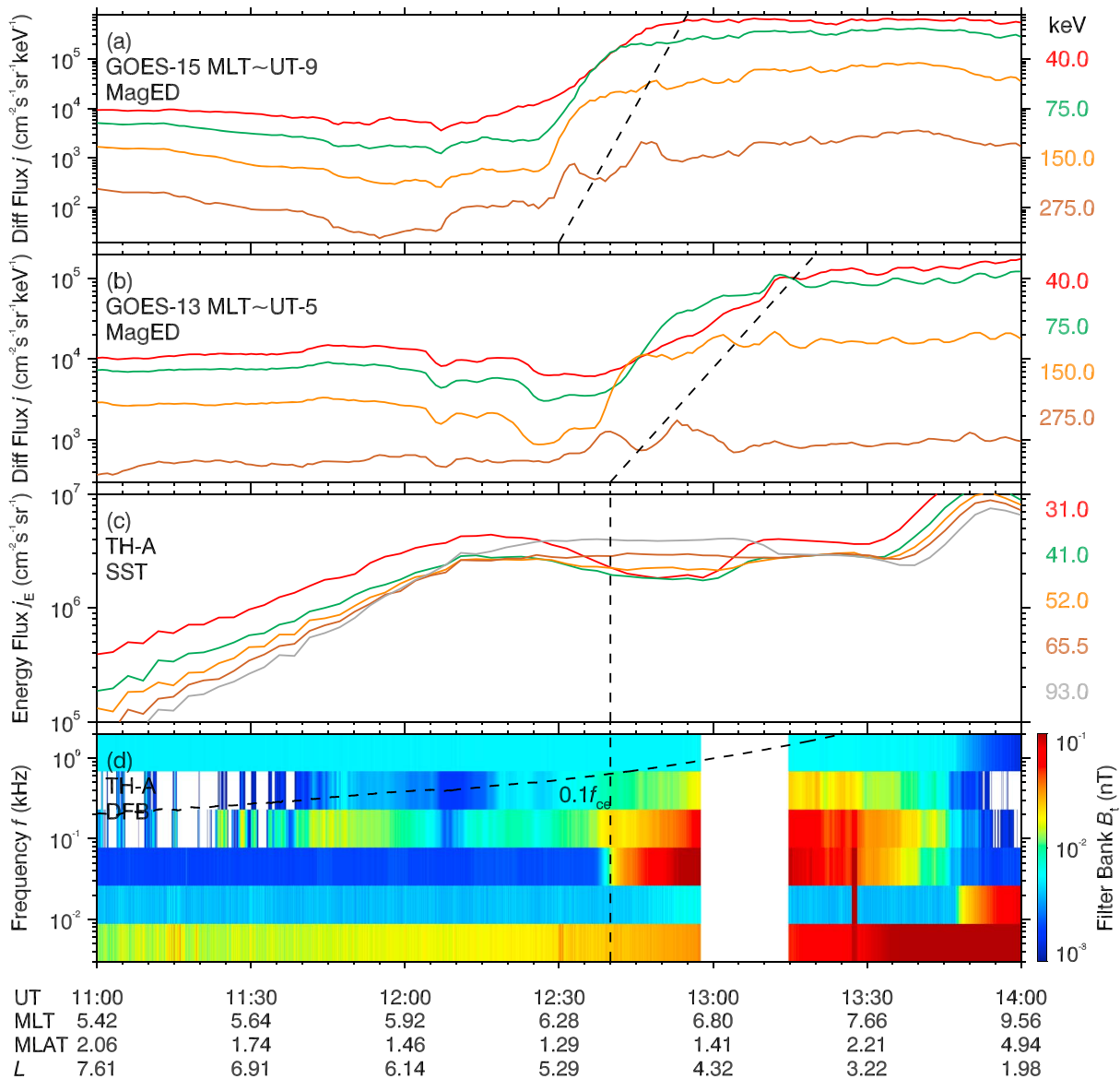
Figure 4. Substorm-injection and magnetospheric waves observed by GOES and THEMIS missions. (a and b) Hot electron differential flux j; (c) hot electron energy flux j_E; (d) wave filter bank amplitude B_t with a data gap around 13:00 UT. In (a) and (b), the oblique-dashed lines help identify the dispersive feature of the substorm injection. In (c) and (d), the vertical-dashed line marks the wave intensification time of TH-A.

Unfortunately, the available data of TH-A did not allow an accurate identification of wave modes. In the plasmasphere, the collected signals above 100 Hz should be the hiss waves, while the magnetosonic waves might partially contribute to the signals below 100 Hz. These observations imply that, along with the azimuthal drift of hot electrons, the plasmaspheric hiss was intensified gradually from nightside to dayside, not supporting the dayside hiss or chorus as a remote source of the enhanced nightside hiss in this event.

4.3. Potential Instability of Substorm-Injected Electrons

Figure 5 illustrates the instability of substorm-injected electrons outside and inside the plasmasphere. As observed by RBSP-A, the substorm-injection front had slightly penetrated into the plasmasphere boundary layer with a steep density gradient. The corresponding whistler-mode waves were excited in the frequency range of 0.1–1.0 kHz, significantly different from the chorus above 1 kHz but similar to the plasmaspheric hiss of RBSP-B. These observations raise the possibility of generation of nightside hiss directly by the substorm-injected electrons in the outer plasmasphere (Meredith et al., 2004; Santolík et al., 2001; Thorne et al., 1979; Tsurutani et al., 2015). Considering that the premidnight plasmapause was found to re-form at
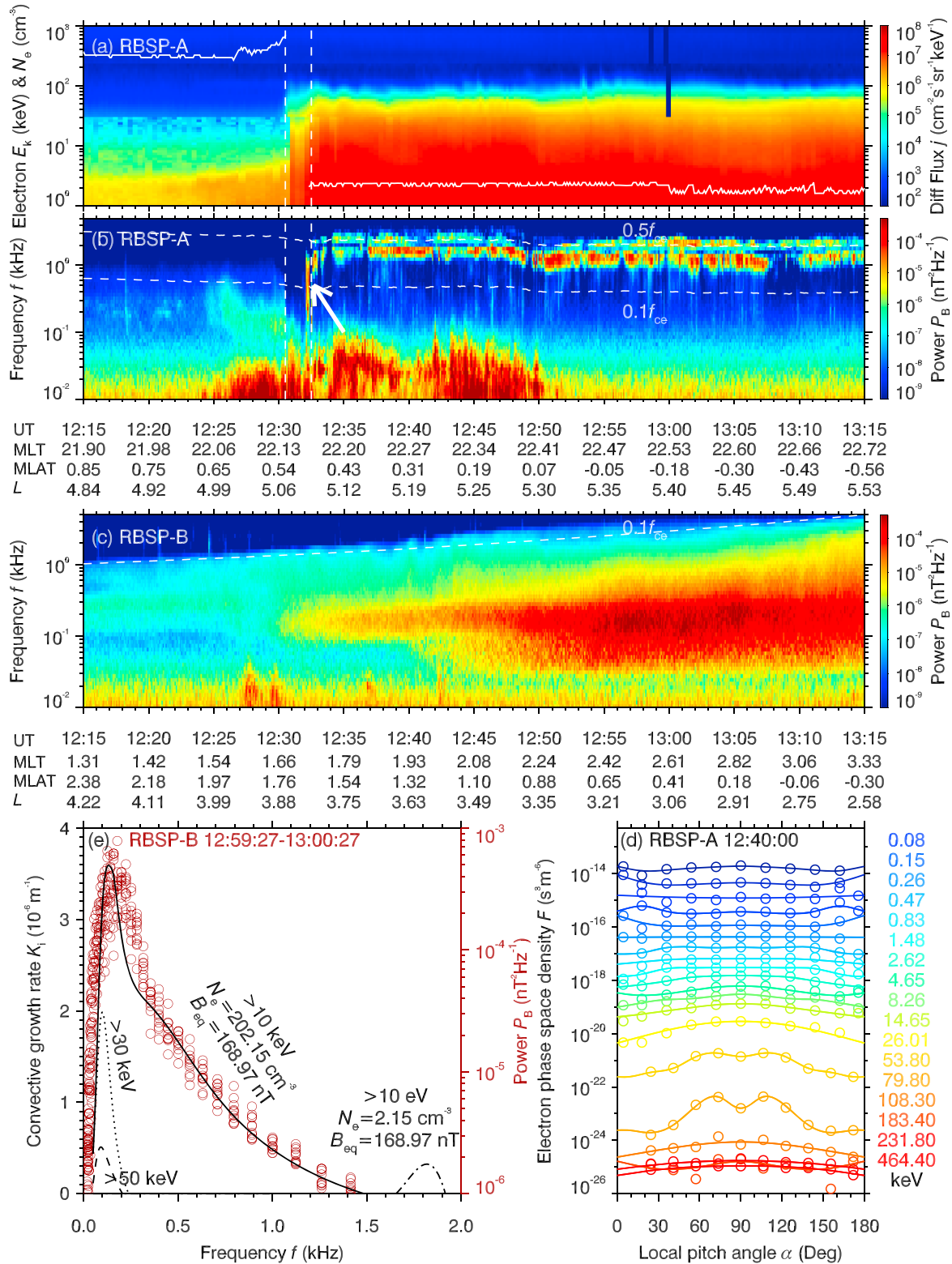
Figure 5. Potential whistler-wave instabilities of injected electrons. (a–c) Zoom-in view of hot electron spin-averaged differential flux j, wave power spectral density P_B, and cold electron density N_e; (d) representative injected electron phase space distribution F depending on pitch angle and energy; (e) hiss wave power P_B (circles) observed by RBSP-B around 13:00 UT and linear growth rate K_i of parallel-propagating whistler waves (lines) driven by electrons with different energies in the low- and high-density region. In (a) and (b), two vertical-dashed lines mark the plasmasphere boundary layer with a sharp density variation.

L_{pp} = 5.1 and that the measured hiss intensification was located at MLT = 01:40–04:00, we can expect the source electrons crossing the postmidnight plasmasphere outside $L \approx 5.1$ (marked by the oblique line shadow in Figure 1b). After the substorm (Figure 1c), the injected hot electrons remained outside the eroded plasmasphere $L_{pp} \approx 4.5$, causing the hiss waves to fall back to the quiet-time level.

The magnetospheric whistler-mode waves usually have peak growth rates around the equator. We here adopt the previously developed code (Liu et al., 2018, 2018; Su et al., 2018) to calculate the linear growth rates of the parallel-propagating whistlers at the equator. The main inputs are the electron phase space density F, the equatorial magnetic field strength B_{eq}, and the cold electron density N_e. Without loss of generality, we select the RBSP-A data around 12:40 UT for the following instability analysis. The electron phase space density was fitted by a smooth cubic spline (Reinsch, 1967) at each energy channel. On the basis of the local observation and the TS04 geomagnetic model (Tsyganenko & Sitnov, 2005), the equatorial magnetic field is set to be B_{eq} = 168.97 nT. Under the low-density (N_e = 2.15 cm^{-3}) condition, the whistler waves are allowed to grow in the frequency range of 1.6–2.0 kHz, qualitatively explaining the occurrence of lower-band chorus. Considering the energy-dispersive feature of the electron injection in the postmidnight sector (Figure 4a), we have analyzed the instabilities of hot electrons in three different energy ranges (>50, >30, and >10 keV) under the high-density (N_e = 202.15 cm^{-3}) condition. The >50-keV electrons can destabilize whistler waves in the frequency range of 80–300 Hz with the peak growth rate of K_i = 0.5 × 10^{-6} m^{-1}, roughly accounting for the plasmaspheric hiss during 12:30–12:40 UT. As time went on, lower energy electrons gradually drifted into the postmidnight sector, yielding the larger wave growth rates over a wider frequency range. For >10-keV electrons, the peak growth rate increases to K_i = 3.5 × 10^{-6} m^{-1}, and the instability frequency range is expanded to 80–1,500 Hz. This growth rate displays the consistent frequency-dependence characteristics to the most significant plasmaspheric hiss power around 13:00 UT. The obtained result is robust to the model specification, as shown in Figure S1. Previous ray-tracing simulations (Chen et al., 2014) have demonstrated that these freshly created hiss waves can further propagate to the inner plasmasphere. The hiss waves launched with parallel normal angles will become oblique far away from the equator but always return back to the quasi-parallel direction near the equator (Chen et al., 2014), consistent with the observed wave propagation characteristics in this event (Figure 2j). These observations and simulations indicate that the substorm-enhanced nightside hiss could result from the instability of hot electrons drifting into the outer plasmasphere.

In the frequency-time spectra of chorus, there were clear rising tones on a timescale of 0.1 s (Figure 3f). The noisy band of plasmaspheric hiss could be interpreted as a superposition of many short-lived (~10 ms) rising and falling tones (Summers et al., 2014). These discrete structures have been considered the manifestations of nonlinear amplification processes (Omura et al., 2008, 2015). Contrary to the predication of linear theory (Figure 5e), the nonlinear amplification rate of chorus in the low-density plasmatrough is much larger than that of hiss in the high-density plasmasphere (Omura et al., 2015). However, different from the poleward propagating chorus, the hiss undergoing cyclic raypaths can be amplified repeatedly in the outer plasmasphere (Chen et al., 2014; Thorne et al., 1979). A combination of these processes (linear instability, nonlinear amplification, and cumulative growth) may explain the comparable amplitudes (~1 nT) of hiss and chorus waveforms (Figures 3c and 3e) in this event. As discussed by Su et al. (2018), even without the repeated growth, the joint action of linear instability and nonlinear amplification in the dayside plasmaspheric plume could produce the poleward-propagating large-amplitude (up to 1.5 nT) hiss.

5. Summary

Using data from seven spacecraft of RBSP, GOES, and THEMIS missions, we examine the generation of nightside plasmaspheric hiss during a substorm on 16 December 2016. Before the substorm, the weak hiss waves (with instantaneous peak amplitudes <40 pT) occurred in the nightside plasmasphere extending to the geosynchronous orbit. During the substorm injection, the nightside plasmasphere was peeled off, and the strong chorus waves were excited outside the newly formed plasmapause L_{pp} = 5.1. At the same time, the intense hiss waves (with instantaneous peak amplitudes 0.9 nT) arose in the inner postmidnight plasmasphere free from the substorm injection. After the substorm, the hiss waves fell back to the quiet-time level in the further eroded plasmasphere $L_{pp} \approx 4.5$.

Within the locally unchanged plasma, the substorm-enhanced hiss waves must originate from other spatial regions. The large-amplitude (up to 0.9 nT) nightside hiss was unlikely to be linked to the nightside chorus suffering strong Landau damping at higher latitudes (Bortnik et al., 2008). The relative timing of dayside and

nightside hiss intensifications did not support the dayside chorus/hiss as a main source of the nightside hiss (Chen et al., 2009). Our data and modeling suggest that the nightside hiss was generated by the hot electrons drifting into the outer plasmasphere and then propagated to the inner plasmasphere (Chen et al., 2014; Meredith et al., 2004; Santolík et al., 2001; Thorne et al., 1979). This scenario can qualitatively explain the temporal evolution, the frequency dependence, and the propagation feature of plasmaspheric hiss observed during this substorm. Its generality is demonstrated by the additional event studies in Figures S2 and S3.

References

Abel, B., & Thorne, R. M. (1998). Electron scattering loss in Earth's inner magnetosphere 1. Dominant physical processes. *Journal of Geophysical Research*, *103*(A2), 2385–2396. https://doi.org/10.1029/97JA02919

Albert, J. M. (1994). Quasi-linear pitch angle diffusion coefficients: Retaining high harmonics quasi-linear pitch angle diffusion coefficients: Retaining high harmonics. *Journal of Geophysical Research*, *99*(A12), 23,741–23,745. https://doi.org/10.1029/94JA02345

Angelopoulos, V. (2008). The THEMIS mission. *Space Science Reviews*, *141*, 5–34. https://doi.org/10.1007/s11214-008-9336-1

Auster, H. U., Glassmeier, K. H., Magnes, W., Aydogar, O., Baumjohann, W., Constantinescu, D., & Wiedemann, M. (2008). The THEMIS fluxgate magnetometer. *Space Science Reviews*, *141*, 235–264. https://doi.org/10.1007/s11214-008-9365-9

Blake, J. B., Carranza, P. A., Claudepierre, S. G., Clemmons, J. H., Crain, W. R., Dotan, Y., & Zakrzewski, M. P. (2013). The Magnetic Electron Ion Spectrometer (MagEIS) instruments aboard the Radiation Belt Storm Probes (RBSP) Spacecraft. *Space Science Reviews*, *179*, 383–421. https://doi.org/10.1007/s11214-013-9991-8

Bortnik, J., Li, W., Thorne, R. M., Angelopoulos, V., Cully, C., Bonnell, J., & Roux, A. (2009). An observation linking the origin of plasmaspheric hiss to discrete chorus emissions. *Science*, *324*, 775–778. https://doi.org/10.1126/science.1171273

Bortnik, J., Thorne, R. M., & Meredith, N. P. (2008). The unexpected origin of plasmaspheric hiss from discrete chorus emissions. *Nature*, *452*, 62–66. https://doi.org/10.1038/nature06741

Breneman, A., Halford, A., Millan, R., McCarthy, M., Fennell, J., Sample, J., & Kletzing, C. (2015). Global-scale coherence modulation of radiation-belt electron loss from plasmaspheric hiss. *Nature*, *523*, 193–195. https://doi.org/10.1038/nature14515

Carpenter, D. L., & Anderson, R. R. (1992). An ISEE/whistler model of equatorial electron density in the magnetosphere. *Journal of Geophysical Research*, *97*, 1097–1108.

Cattell, C., Wygant, J. R., Goetz, K., Kersten, K., Kellogg, P. J., von Rosenvinge, T., & Russell, C. T. (2008). Discovery of very large amplitude whistler-mode waves in Earth's radiation belts. *Geophysical Research Letters*, *35*, L01105. https://doi.org/10.1029/2007GL032009

Chappell, C. R. (1974). Detached plasma regions in the magnetosphere. *Journal of Geophysical Research*, *79*(13), 1861–1870. https://doi.org/10.1029/JA079i013p01861

Chen, L., Bortnik, J., Thorne, R. M., Horne, R. B., & Jordanova, V. K. (2009). Three-dimensional ray tracing of VLF waves in a magnetospheric environment containing a plasmaspheric plume. *Geophysical Research Letters*, *36*, L22101. https://doi.org/10.1029/2009GL040451

Chen, L., Thorne, R. M., Bortnik, J., Li, W., Horne, R. B., Reeves, G. D., & Fennell, J. F. (2014). Generation of unusually low frequency plasmaspheric hiss. *Geophysical Research Letters*, *41*, 5702–5709. https://doi.org/10.1002/2014GL060628

Cornilleau-Wehrlin, N., Solomon, J., Korth, A., & Kremser, G. (1993). Generation mechanism of plasmaspheric ELF/VLF hiss: A statistical study from GEOS 1 data. *Journal of Geophysical Research*, *98*(A12), 21,471–21,479. https://doi.org/10.1029/93JA01919

Cully, C. M., Bonnell, J. W., & Ergun, R. E. (2008). THEMIS observations of long-lived regions of large-amplitude whistler waves in the inner magnetosphere. *Geophysical Research Letters*, *35*, L17S16. https://doi.org/10.1029/2008GL033643

Cully, C. M., Ergun, R. E., Stevens, K., Nammari, A., & Westfall, J. (2008). The THEMIS digital fields board. *Space Science Reviews*, *141*, 343–355. https://doi.org/10.1007/s11214-008-9417-1

Davis, G. K. (2007). History of the NOAA satellite program. *Journal of Applied Remote Sensing*, *1*, 12504.

Draganov, A. B., Inan, U. S., Sonwalkar, V. S., & Bell, T. F. (1992). Magnetospherically reflected whistlers as a source of plasmaspheric hiss. *Geophysical Research Letters*, *19*(3), 233–236. https://doi.org/10.1029/91GL03167

Falkowski, B. J., Tsurutani, B. T., Lakhina, G. S., & Pickett, J. S. (2017). Two sources of dayside intense, quasi-coherent plasmaspheric hiss: A new mechanism for the slot region? *Journal of Geophysical Research: Space Physics*, *122*, 1643–1657. https://doi.org/10.1002/2016JA023289

Friedel, R. H. W., Korth, H., Henderson, M. G., Thomsen, M. F., & Scudder, J. D. (2001). Plasma sheet access to the inner magnetosphere. *Journal of Geophysical Research*, *106*(A4), 5845–5858. https://doi.org/10.1029/2000JA003011

Friedel, R. H. W., Korth, A., & Kremser, G. (1996). Substorm onsets observed by CRRES: Determination of energetic particle source regions. *Journal of Geophysical Research*, *101*(A6), 13,137–13,154. https://doi.org/10.1029/96JA00399

Funsten, H. O., Skoug, R. M., Guthrie, A. A., MacDonald, E. A., Baldonado, J. R., Harper, R. W., & Chen, J. (2013). Helium, Oxygen, Proton, and Electron (HOPE) mass spectrometer for the Radiation Belt Storm Probes mission. *Space Science Reviews*, *179*, 423–484. https://doi.org/10.1007/s11214-013-9968-7

GOES N Series Data Book (2009). Revision C, Boeing Satellite Systems Inc.

Gao, Z., Su, Z., Zhu, H., Xiao, F., Zheng, H., Wang, Y., & Wang, S. (2016). Intense low-frequency chorus waves observed by Van Allen Probes: Fine structures and potential effect on radiation belt electrons. *Geophysical Research Letters*, *43*, 967–977. https://doi.org/10.1002/2016GL067687

Goldstein, J., Sandel, B. R., Thomsen, M. F., Spasojević, M., & Reiff, P. H. (2004). Simultaneous remote sensing and in situ observations of plasmaspheric drainage plumes. *Journal of Geophysical Research*, *109*, A03202. https://doi.org/10.1029/2003JA010281

Green, J. L., Boardsen, S., Garcia, L., Taylor, W. W. L., Fung, S. F., & Reinisch, B. W. (2005). On the origin of whistler mode radiation in the plasmasphere. *Journal of Geophysical Research*, *110*, A03201. https://doi.org/10.1029/2004JA010495

He, Z., Yan, Q., Chu, Y., & Cao, Y. (2016). Wave-driven gradual loss of energetic electrons in the slot region. *Journal of Geophysical Research: Space Physics*, *121*, 8614–8623. https://doi.org/10.1002/2016JA023087

Horne, R. B., Thorne, R. M., Glauert, S. A., Meredith, N. P., Pokhotelov, D., & Santolík, O. (2007). Electron acceleration in the Van Allen radiation belts by fast magnetosonic waves. *Geophysical Research Letters*, *34*, L17107. https://doi.org/10.1029/2007GL030267

Horwitz, J. L., Comfort, R. H., & Chappell, C. R. (1990). A statistical characterization of plasmasphere density structure and boundary locations. *Journal of Geophysical Research*, *95*(A6), 7937–7947. https://doi.org/10.1029/JA095iA06p07937

Kellogg, P., Cattell, C., Goetz, K., Monson, S., & Wilson, L. (2011). Large amplitude whistlers in the magnetosphere observed with Wind-Waves. *Journal of Geophysical Research*, *116*, A09224. https://doi.org/10.1029/2010JA015919

King, J. H., & Papitashvili, N. E. (2005). Solar wind spatial scales in and comparisons of hourly Wind and ACE plasma and magnetic field data. *Journal of Geophysical Research*, *110*, A02104. https://doi.org/10.1029/2004JA010649

Kletzing, C. A., Kurth, W. S., Acuna, M., MacDowall, R. J., Torbert, R. B., Averkamp, T., & Tyler, J. (2013). The Electric and Magnetic Field Instrument Suite and Integrated Science (EMFISIS) on RBSP. *Space Science Reviews*, *179*, 127–181. https://doi.org/10.1007/s11214-013-9993-6

Kurth, W. S., Pascuale, S. D., Faden, J. B., Kletzing, C. A., Hospodarsky, G. B., Thaller, S., & Wygant, J. R. (2014). Electron densities inferred from plasma wave spectra obtained by the waves instrument on Van Allen Probes. *Journal of Geophysical Research: Space Physics*, *120*, 904–914. https://doi.org/10.1002/2014JA020857

Laakso, H., Santolik, O., Horne, R., Kolmasová, I., Escoubet, P., Masson, A., & Taylor, M. (2015). Identifying the source region of plasmaspheric hiss. *Geophysical Research Letters*, *42*, 3141–3149. https://doi.org/10.1002/2015GL063755

Lemaire, J. F., & Gringauz, K. I. (1998). *The Earth's plasmasphere*. Cambridge, UK: Cambridge University Press.

Li, W., Chen, L., Bortnik, J., Thorne, R. M., Angelopoulos, V., Kletzing, C. A., & Hospodarsky, G. B. (2015). First evidence for chorus at a large geocentric distance as a source of plasmaspheric hiss: Coordinated THEMIS and Van Allen Probes observation. *Geophysical Research Letters*, *42*, 241–248. https://doi.org/10.1002/2014GL062832

Li, W., Ma, Q., Thorne, R. M., Bortnik, J., Kletzing, C. A., Kurth, W. S., & Nishimura, Y. (2015). Statistical properties of plasmaspheric hiss derived from Van Allen Probes data and their effects on radiation belt electron dynamics. *Journal of Geophysical Research: Space Physics*, *120*, 3393–3405. https://doi.org/10.1002/2015JA021048

Li, W., Thorne, R. M., Angelopoulos, V., Bortnik, J., Cully, C. M., Ni, B., & Magnes, W. (2009). Global distribution of whistler-mode chorus waves observed on the THEMIS spacecraft. *Geophysical Research Letters*, *36*, L09104. https://doi.org/10.1029/2009GL037595

Li, W., Thorne, R. M., Bortnik, J., Nishimura, Y., Angelopoulos, V., Chen, L., & Bonnell, J. W. (2010). Global distributions of suprathermal electrons observed on THEMIS and potential mechanisms for access into the plasmasphere. *Journal of Geophysical Research*, *115*, A00J10. https://doi.org/10.1029/2010JA015687

Li, W., Thorne, R. M., Bortnik, J., Reeves, G. D., Kletzing, C. A., Kurth, W. S., & Thaller, S. A. (2013). An unusual enhancement of low-frequency plasmaspheric hiss in the outer plasmasphere associated with substorm-injected electrons. *Geophysical Research Letters*, *40*, 3798–3803. https://doi.org/10.1002/grl.50787

Liu, N., Su, Z., Gao, Z., Reeves, G. D., Zheng, H., Wang, Y., & Wang, S. (2017). Shock-induced disappearance and subsequent recovery of plasmaspheric hiss: Coordinated observations of RBSP, THEMIS, and POES satellites. *Journal of Geophysical Research: Space Physics*, *122*, 10,421–10,435. https://doi.org/10.1002/2017JA024470

Liu, N., Su, Z., Gao, Z., Zheng, H., Wang, Y., Wang, S., & Wygant, J. R. (2017). Simultaneous disappearances of plasmaspheric hiss, exohiss and chorus waves triggered by a sudden decrease in solar wind dynamic pressure. *Geophysical Research Letters*, *43*, 52–61. https://doi.org/10.1002/2016GL071987

Liu, N., Su, Z., Zheng, H., Wang, Y., & Wang, S. (2018). Magnetosonic harmonic falling and rising frequency emissions potentially generated by nonlinear wave-wave interactions in the Van Allen radiation belts. *Geophysical Research Letters*, *45*, 7985–7995. https://doi.org/10.1029/2018GL079232

Liu, N., Su, Z., Zheng, H., Wang, Y., & Wang, S. (2018). Prompt disappearance and emergence of radiation belt magnetosonic waves induced by solar wind dynamic pressure variations. *Geophysical Research Letters*, *45*, 585–594. https://doi.org/10.1002/2017GL076382

Lyons, L. R., & Thorne, R. M. (1973). Equilibrium structure of radiation belt electrons. *Journal of Geophysical Research*, *78*(13), 2142–2149. https://doi.org/10.1029/JA078i013p02142

Malaspina, D. M., Jaynes, A. N., Boulé, C., Bortnik, J., Thaller, S. A., Ergun, R. E., & Wygant, J. R. (2016). The distribution of plasmaspheric hiss wave power with respect to plasmapause location. *Geophysical Research Letters*, *43*, 7878–7886. https://doi.org/10.1002/2016GL069982

Malaspina, D. M., Jaynes, A. N., Hospodarsky, G., Bortnik, J., Ergun, R. E., & Wygant, J. (2017). Statistical properties of low-frequency plasmaspheric hiss. *Journal of Geophysical Research: Space Physics*, *122*, 8340–8352. https://doi.org/10.1002/2017JA024328

Mauk, B. H., Fox, N. J., Kanekal, S. G., Kessel, R. L., Sibeck, D. G., & Ukhorskiy, A. (2013). Science objectives and rationale for the Radiation Belt Storm Probes mission. *Space Science Reviews*, *179*, 3–27. https://doi.org/10.1007/s11214-012-9908-y

McFadden, J. P., Carlson, C. W., Larson, D., Bonnell, J., Mozer, F., Angelopoulos, V., & Auster, U. (2008). THEMIS ESA first science results and performance issues. *Space Science Reviews*, *141*, 477–508. https://doi.org/10.1007/s11214-008-9433-1

McIlwain, C. E. (1974). Substorm injection boundaries. In B. M. McCormac (Ed.), *Magnetospheric physics* (pp. 143–154). Astrophysics and Space Science Library. UK: Springer Netherlands.

Meredith, N. P., Horne, R. B., Bortnik, J., Thorne, R. M., Chen, L., Li, W., & Sicard-Piet, A. (2013). Global statistical evidence for chorus as the embryonic source of plasmaspheric hiss. *Geophysical Research Letters*, *40*, 2891–2896. https://doi.org/10.1002/grl.50593

Meredith, N. P., Horne, R. B., Glauert, S., & Anderson, R. R. (2007). Slot region electron loss timescales due to plasmaspheric hiss and lightning-generated whistlers. *Journal of Geophysical Research*, *112*, A08214. https://doi.org/10.1029/2007JA012413

Meredith, N. P., Horne, R. B., Kersten, T., Li, W., Bortnik, J., Sicard, A., & Yearby, K. H. (2018). Global model of plasmaspheric hiss from multiple satellite observations. *Journal of Geophysical Research: Space Physics*, *123*, 4526–4541. https://doi.org/10.1029/2018JA025226

Meredith, N. P., Horne, R. B., Thorne, R. M., Summers, D., & Anderson, R. R. (2004). Substorm dependence of plasmaspheric hiss. *Journal of Geophysical Research*, *109*, A06209. https://doi.org/10.1029/2004JA010387

Mourenas, D., & Ripoll, J. F. (2012). Analytical estimates of quasi-linear diffusion coefficients and electron lifetimes in the inner radiation belt. *Journal of Geophysical Research*, *117*, A01204. https://doi.org/10.1029/2011JA016985

Ni, B., Bortnik, J., Thorne, R. M., Ma, Q., & Chen, L. (2013). Resonant scattering and resultant pitch angle evolution of relativistic electrons by plasmaspheric hiss. *Journal of Geophysical Research: Space Physics*, *118*, 7740–7751. https://doi.org/10.1002/2013JA019260

Ni, B., Hua, M., Zhou, R., Yi, J., & Fu, S. (2017). Competition between outer zone electron scattering by plasmaspheric hiss and magnetosonic waves. *Geophysical Research Letters*, *44*, 3465–3474. https://doi.org/10.1002/2017GL072989

Ni, B., Li, W., Thorne, R. M., Bortnik, J., Ma, Q., Chen, L., & Claudepierre, S. G. (2014). Resonant scattering of energetic electrons by unusual low-frequency hiss. *Geophysical Research Letters*, *41*, 1854–1861. https://doi.org/10.1002/2014GL059389

Nishida, A. (1966). Formation of plasmapause, or magnetospheric plasma knee, by the combined action of magnetospheric convection and plasma escape from the tail. *Journal of Geophysical Research*, *71*(23), 5669–5679. https://doi.org/10.1029/JZ071i023p05669

Omura, Y., Katoh, Y., & Summers, D. (2008). Theory and simulation of the generation of whistler-mode chorus. *Journal of Geophysical Research*, *113*, A04223. https://doi.org/10.1029/2007JA012622

Omura, Y., Nakamura, S., Kletzing, C. A., Summers, D., & Hikishima, M. (2015). Nonlinear wave growth theory of coherent hiss emissions in the plasmasphere. *Journal of Geophysical Research: Space Physics*, *120*, 7642–7657. https://doi.org/10.1002/2015JA021520

Pierrard, V., Khazanov, G. V., Cabrera, J., & Lemaire, J. (2008). Influence of the convection electric field models on predicted plasmapause positions during magnetic storms. *Journal of Geophysical Research*, *113*, A08212. https://doi.org/10.1029/2007JA012612

Reeves, G. D., Fritz, T. A., Cayton, T. E., & Belian, R. D. (1990). Multi-satellite measurements of the substorm injection region. *Geophysical Research Letters*, *17*(11), 2015–2018. https://doi.org/10.1029/GL017i011p02015

Reinsch, C. H. (1967). Smoothing by spline functions. *Numerische Mathematik*, *10*(3), 177–183.

Russell, C. T., Holzer, R. E., & Smith, E. J. (1969). OGO 3 observations of ELF noise in the magnetosphere. 1. Spatial extent and frequency of occurrence. *Journal of Geophysical Research*, *74*(3), 755–777. https://doi.org/10.1029/JA074i003p00755

Santolík, O., & Chum, J. (2009). The origin of plasmaspheric hiss. *Science*, *324*, 729–730. https://doi.org/10.1126/science.1172878

Santolík, O., Kletzing, C., Kurth, W., Hospodarsky, G., & Bounds, S. (2014). Fine structure of large-amplitude chorus wave packets. *Geophysical Research Letters*, *41*, 293–299. https://doi.org/10.1002/2013GL058889

Santolík, O., Parrot, M., & Lefeuvre, F. (2003). Singular value decomposition methods for wave propagation analysis. *Radio Science*, *38*(1), 1010. https://doi.org/10.1029/2000RS002523

Santolík, O., Parrot, M., Storey, L. R. O., Pickett, J. S., & Gurnett, D. A. (2001). Propagation analysis of plasmaspheric hiss using Polar PWI measurements. *Geophysical Research Letters*, *28*(6), 1127–1130. https://doi.org/10.1029/2000GL012239

Santolík, O., Pickett, J. S., Gurnett, D. A., Menietti, J. D., Tsurutani, B. T., & Verkhoglyadova, O. (2010). Survey of Poynting flux of whistler mode chorus in the outer zone. *Journal of Geophysical Research*, *115*, A00F13. https://doi.org/10.1029/2009JA014925

Santolík, O., Pickett, J. S., Gurnett, D. A., & Storey, L. R. O. (2002). Magnetic component of narrowband ion cyclotron waves in the auroral zone. *Journal of Geophysical Research*, *107*(A12), 1444. https://doi.org/10.1029/2001JA000146

Shprits, Y. Y., Chen, L., Ukhorskiy, A., & Thorne, R. (2009). Simulations of pitch-angle scattering of relativistic electrons with mlt-dependent diffusion coefficients. *Journal of Geophysical Research*, *114*, A03219. https://doi.org/10.1029/2008JA013695

Solomon, J., Cornilleau-Wehrlin, N., Korth, A., & Kremser, G. (1988). An experimental study of ELF/VLF hiss generation in the Earth's magnetosphere. *Journal of Geophysical Research*, *93*(A3), 1839–1847. https://doi.org/10.1029/JA093iA03p01839

Sonwalkar, V. S., & Inan, U. S. (1989). Lightning as an embryonic source of VLF hiss. *Journal of Geophysical Research*, *94*(A6), 6986–6994. https://doi.org/10.1029/JA094iA06p06986

Spence, H. E., Reeves, G. D., Baker, D. N., Blake, J. B., Bolton, M., Bourdarie, S., & Thorne, R. M. (2013). Science goals and overview of the Energetic Particle, Composition, and Thermal Plasma (ECT) suite on NASA's Radiation Belt Storm Probes (RBSP) mission. *Space Science Reviews*, *179*, 311–336. https://doi.org/10.1007/s11214-013-0007-5

Su, Z., Gao, Z., Zhu, H., Li, W., Zheng, H., Wang, Y., & Wygant, J. R. (2016). Nonstorm time dropout of radiation belt electron fluxes on 24 September 2013. *Journal of Geophysical Research: Space Physics*, *121*, 6400–6416. https://doi.org/10.1002/2016JA022546

Su, Z., Liu, N., Zheng, H., Wang, Y., & Wang, S. (2018). Large-amplitude extremely low frequency hiss waves in plasmaspheric plumes. *Geophysical Research Letters*, *45*, 565–577. https://doi.org/10.1002/2017GL076754

Su, Z., Wang, G., Liu, N., Zheng, H., Wang, Y., & Wang, S. (2017). Direct observation of generation and propagation of magnetosonic waves following substorm injection. *Geophysical Research Letters*, *44*, 7587–7597. https://doi.org/10.1002/2017GL074362

Su, Z., Zhu, H., Xiao, F., Zheng, H., Wang, Y., Shen, C., et al. (2015). Disappearance of plasmaspheric hiss following interplanetary shock. *Geophysical Research Letters*, *42*, 3129–3140. https://doi.org/10.1002/2015GL063906

Summers, D., Ni, B., & Meredith, N. P. (2007). Timescales for radiation belt electron acceleration and loss due to resonant wave-particle interactions: 2. Evaluation for VLF chorus, ELF hiss, and electromagnetic ion cyclotron waves. *Journal of Geophysical Research*, *112*, A04207. https://doi.org/10.1029/2006JA011993

Summers, D., Ni, B., Meredith, N. P., Horne, R. B., Thorne, R. M., Moldwin, M. B., & Anderson, R. R. (2008). Electron scattering by whistler-mode ELF hiss in plasmaspheric plumes. *Journal of Geophysical Research*, *113*, A04219. https://doi.org/10.1029/2007JA012678

Summers, D., Omura, Y., Nakamura, S., & Kletzing, C. A. (2014). Fine structure of plasmaspheric hiss. *Journal of Geophysical Research: Space Physics*, *119*, 9134–9149. https://doi.org/10.1002/2014JA020437

Thorne, R. M., Church, S. R., & Gorney, D. J. (1979). On the origin of plasmaspheric hiss: The importance of wave propagation and the plasmapause. *Journal of Geophysical Research*, *84*(A9), 5241–5247. https://doi.org/10.1029/JA084iA09p05241

Thorne, R. M., Li, W., Ni, B., Ma, Q., Bortnik, J., Baker, D. N., et al. (2013). Evolution and slow decay of an unusual narrow ring of relativistic electrons near $L \sim 3.2$ following the September 2012 magnetic storm. *Geophysical Research Letters*, *40*, 3507–3511. https://doi.org/10.1002/grl.50627

Thorne, R. M., Smith, E. J., Burton, R. K., & Holzer, R. E. (1973). Plasmaspheric hiss. *Journal of Geophysical Research*, *78*(10), 1581–1596. https://doi.org/10.1029/JA078i010p01581

Tsurutani, B. T., Falkowski, B. J., Pickett, J. S., Santolik, O., & Lakhina, G. S. (2015). Plasmaspheric hiss properties: Observations from Polar. *Journal of Geophysical Research: Space Physics*, *120*, 414–431. https://doi.org/10.1002/2014JA020518

Tsurutani, B. T., Falkowski, B. J., Verkhoglyadova, O. P., Pickett, J. S., Santolík, O., & Lakhina, G. S. (2012). Dayside ELF electromagnetic wave survey: A Polar statistical study of chorus and hiss. *Journal of Geophysical Research*, *117*, A00L12. https://doi.org/10.1029/2011JA017180

Tsyganenko, N. A., & Sitnov, M. I. (2005). Modeling the dynamics of the inner magnetosphere during strong geomagnetic storms. *Journal of Geophysical Research*, *110*, A03208. https://doi.org/10.1029/2004JA010798

Wang, C., Zong, Q., Xiao, F., Su, Z., Wang, Y., & Yue, C. (2011). The relations between magnetospheric chorus and hiss inside and outside the plasmasphere boundary layer: Cluster observation. *Journal of Geophysical Research*, *116*, A07221. https://doi.org/10.1029/2010JA016240

Wilson, L., Cattell, C., Kellogg, P., Wygant, J., Goetz, K., Breneman, A., & Kersten, K. (2011). The properties of large amplitude whistler mode waves in the magnetosphere: Propagation and relationship with geomagnetic activity. *Geophysical Research Letters*, *38*, L17107. https://doi.org/10.1029/2011GL048671

Yue, C., Chen, L., Bortnik, J., Ma, Q., Thorne, R. M., Angelopoulos, V., & Spence, H. E. (2017). The characteristic response of whistler mode waves to interplanetary shocks. *Journal of Geophysical Research: Space Physics*, *122*, 10,047–10,057. https://doi.org/10.1002/2017JA024574